Image Rectification with the Pinax Camera Model in Underwater Stereo Systems with Verged Cameras

Conference Paper · September 2017

CITATION
1

READS
327

3 authors:

Tomasz Łuczyński
Heriot-Watt University
10 PUBLICATIONS **45** CITATIONS
SEE PROFILE

Max Pfingsthorn
OFFIS
66 PUBLICATIONS **695** CITATIONS
SEE PROFILE

Andreas Birk
Jacobs University
259 PUBLICATIONS **3,267** CITATIONS
SEE PROFILE

Image Rectification with the Pinax Camera Model in Underwater Stereo Systems with Verged Cameras

Tomasz Łuczyński, Max Pfingsthorn and Andreas Birk
Jacobs University Bremen
School of Engineering and Science
Campus Ring 1, 28759 Bremen, Germany
t.luczynski@jacobs-university.de

***Abstract*— Vision methods are very commonly used in underwater robotics. However, the cameras must be enclosed in a sealed housing for which flat-pane windows are the most economical and hence most popular solution. But they cause non-trivial refraction-based distortions at the air-glass-water interface. Recently, a new model for underwater cameras calibration called Pinax was introduced, which combines aspects of an axial and a pinhole camera model to derive an as accurate as possible and at the same time computational feasible solution. Here it is shown, how the Pinax model can be applied to stereo cameras when two verged cameras are behind a single flat glass panel. Real world experiments under different water conditions show that our method outperforms standard methods using pinhole models in combination with in-water calibration.**

I. Introduction and related work

Underwater vision is a widespread sensing technique for Unmanned Underwater Vehicles (UUV) - both for Remotely Operated Vehicles (ROV) as well as for Autonomous Underwater Vehicles (AUV). The high update rate of cameras, their high resolution, information about color and the variety of relatively cheap cameras in the market are only a few of the major advantages of vision systems. A short discussion of vision systems in underwater robotics is for example given in [1]. The main drawbacks of underwater vision systems are limited range, necessity of good illumination of the observed scene, and the phenomenon of refraction that influences the observed image. Refraction, as the main source of distortion in the image, is the biggest obstacle on the way to the use of common 3D vision algorithms underwater. It can be mitigated by the use of dome ports but they need to be specifically engineered to fit the camera parameters and their integration is non-trivial. Flat-ports are hence very popular but suffer from complex refraction distortions, which are the topic of this paper.

In [2] the errors caused by not compensating the refractive distortions are discussed. They are identified to be significant, however no solution to this problem is proposed. In [3] a mathematical model of underwater imaging through planar glass ports is introduced. Matrices corresponding to fundamental and homography matrices are derived. They however depend on the incident angle of the light ray corresponding to each image pixel, so they cannot be used directly for underwater vision methods. Since no continuation of this work was published, their results remain as theoretical considerations of conceptual value.

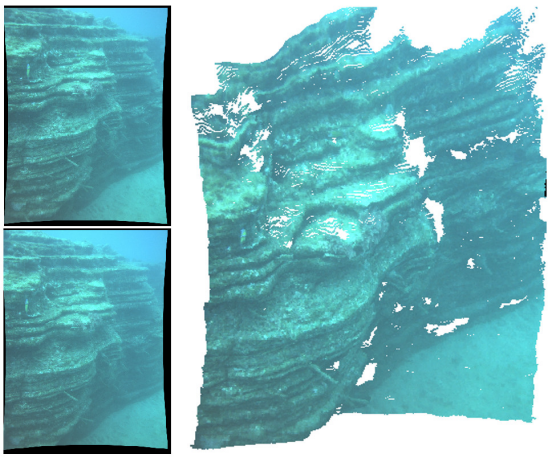

Fig. 1. A 2.5D colored point cloud (right) generated from images (left) from a custom-made underwater stereo camera on the Vortex vehicle of the Institut francais de recherche pour l'exploitation de la mer (Ifremer) where the camera calibration and epipolar image rectification is performed with the method presented in this paper. The data was collected within the EU FP7-funded MORPH project.

Recently a lot of attention was received by [4], where the case of a planar interface with parallel refractive surfaces (e.g., glass panel) is analyzed. The camera behind such a panel is identified to be in fact an axial camera [5], with a line rather than a single point of projection. In [6], a detailed description of refraction effects on this camera model is provided. It is also shown that a camera in a flat pane underwater housing is not a single viewpoint (SVP) camera, i.e., the standard pinhole model cannot be used, respectively leads to inaccurate results. Several papers [7], [8], [9], [10] propose different variations of numerical optimization of the housing parameters using standard calibration patterns, but this requires engineering efforts for the window integration similar to dome ports and can not be applied to off-the-shelf housings. Furthermore, this line of work is using computationally complex methods and it is targeted at offline processing of multi-view data.

In recent own work [11] aspects of the pinhole model with the axial model are combined to derive a novel calibration and epipolar rectification process for underwater cameras that is very fast and very efficient, i.e., a one time calibration in air is sufficient. This calibration method and the new camera

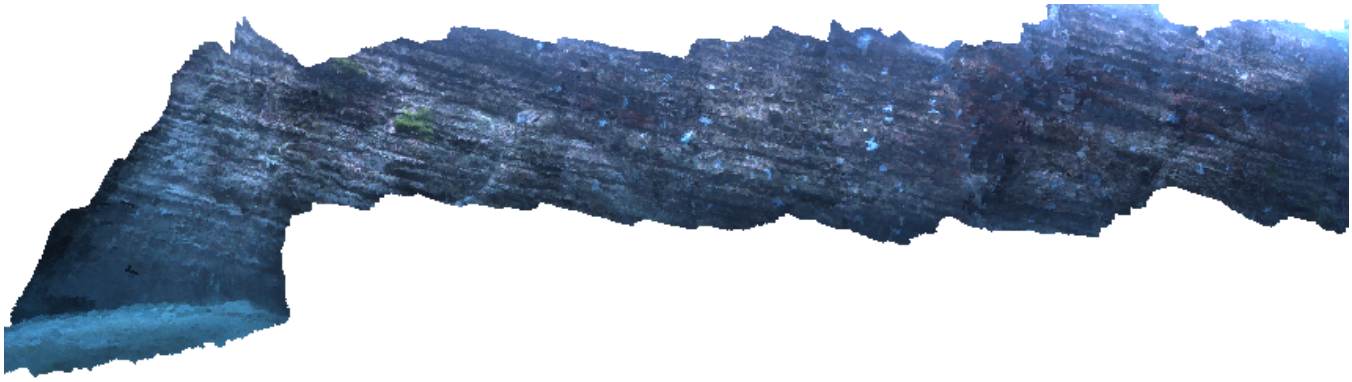

Fig. 2. A 3D map generated from 350 stereo based point clouds from a Bumblebee camera on a Sparus vehicle of the University of Girona where the camera calibration and epipolar image rectification is performed with the method presented in this paper. The data was collected within the EU FP7-funded MORPH project.

model, called Pinax, can be applied to stereo cameras in a straight-forward way if both cameras are in separate housing or if they parallel behind a single flat pane. In this paper the case of a stereo system with verged cameras behind a single flat pane is discussed.

The rest of the paper is structured as follows. In the next two sections the setup parameters of the underwater vision system and their influence on image distortion are discussed. In Sec. IV, the analysis from Sec. II is used to design a camera-housing setup with a flat port where the SVP assumption is valid up to negligible error. Section V presents experiments with real life data validating our method in comparison to the state of the art. Sec. VI concludes the paper.

II. The Pinhole vs. the Flat Refractive Model

A. System Setup

First, we discuss the case of a single camera based on the authors previous own work [11]. The following setup is considered. A physical pinhole camera is enclosed in a water sealed housing with a glass panel through which it observes the underwater environment. This in-air device inside the housing is in the following denoted as the *physical camera*. The glass panel is flat and both sides are parallel. The notations and a schematic view are presented in Fig. 3. If not mentioned otherwise, we use the terms *camera* to denote the overall underwater camera set-up including the window with the air/glass/water interfaces.

B. Theoretical Background

As shown in [4], the physically accurate model of this overall set-up of an underwater camera corresponds to an axial camera. It means that light rays creating the image do not intersect in one point, as in the pinhole model, but they all cross one line, referred to as the axis of the camera. The line segment where the actual light rays intersect is known as the focusing section. This camera geometry can only be approximated with a pinhole model by reducing the focusing section with a point. The conclusion is that the quality of this approximation directly depends on the length of this section.

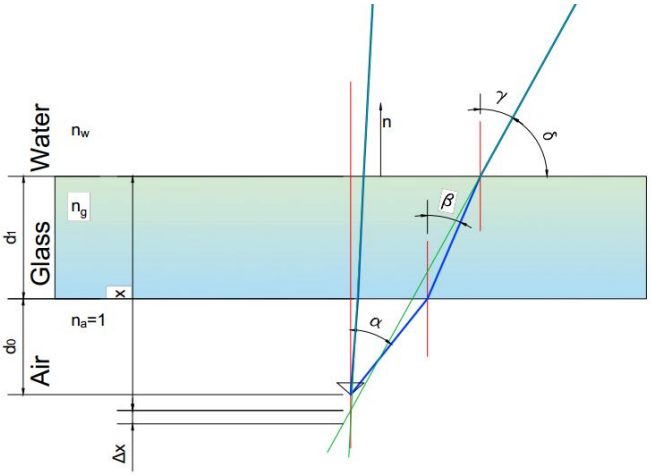

Fig. 3. Schematic view of the setup: d_0 - distance from the center of projection to the glass window, d_1 - thickness of the glass, x - distance to point of intersection of the light ray with the camera axis, Δx - length of the focusing section, n_a, n_g, n_w - refraction indices, scaled so that $n_a = 1$, n - normal vector to the glass surface, α - incident angle. The blue line represents the physically accurate light ray; the green line is the apparent ray traced back to the camera's optical axis.

In the limit case, the pinhole camera is an axial camera where the focusing section of the camera axis is infinitely short. To analyse the mechanism of refraction, ray tracing through the air-glass-water interface and the apparent intersection of the rays in the water with the camera axis can be modeled (Fig. 3):

$$\beta = \arcsin \frac{\sin \alpha}{n_g}$$
$$\gamma = \arcsin \frac{\sin \alpha}{n_w}$$
$$\delta = \frac{\pi}{2} - \gamma$$

For the purpose of these considerations we assume that the refractive plane normal and therefore the camera axis, for the axial model, is parallel to the optical axis of the camera. This assumption is without loss of generality since the incident

angle α, the only parameter related to the physical camera rotation, can easily be adjusted if needed. A fixed offset can simply be added if the physical camera inside the housing is rotated. For the sake of completeness the equations for finding incident angles α when given the physical camera pose in the housing is also noted:

$$v_0 = K^{-1}p$$
$$\alpha = \arccos \frac{v_0^T n}{|v_0||n|}$$

where K is the intrinsic parameter matrix and p represents pixel coordinates on the image.

The focusing distance x (Fig. 3) can be computed as:

$$x = \tan\delta(d_0 \tan\alpha + d_1 \tan\beta)$$

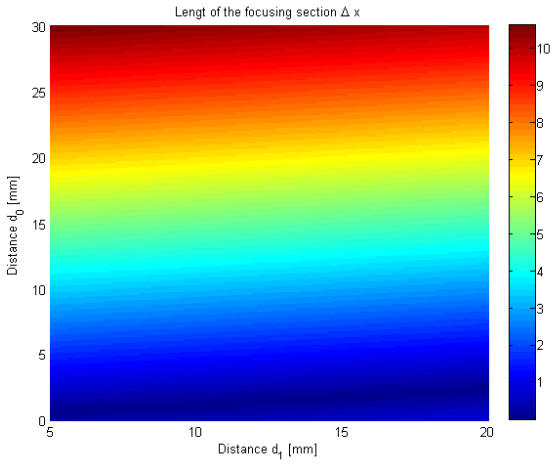

Fig. 4. The length of the focusing section Δx as a function of d_0 and d_1. Note the large minimum region spanning across all values of d_1 on the bottom of the figure.

Fig. 4 shows the length of the focusing section Δx as a function of d_0 and d_1. It illustrates that changes in d_0 are much more significant than in d_1. This is due to the relatively small difference between the refraction index of glass (≈ 1.5) and water (≈ 1.33, [12]) compared to the refraction on the glass-air interface.

Fig. 5 shows where the light rays in water cross the camera's optical axis for different values of d_0. Each line on the graph corresponds to a different incident angle. It can be seen that they never cross the same spot, but for some optimal d_0, they are very close to intersecting in one point.

To find this optimal value the following method is used. The ray tracing is implemented based on the above formulas. Then, a non-linear optimization method is used to minimize the length of the section where light rays backtraced from the water intersect the camera axis. For the case where $d_1 = 10mm$, the glass refraction index $n_g = 1.5$ and the water refraction index $n_w = 1.335$, the method converges for example to $d_0 = 1.4282mm$, where all light rays intersect the optical axis on a section Δx that is only $0.0079mm$ long. The result allows to define the middle of this section

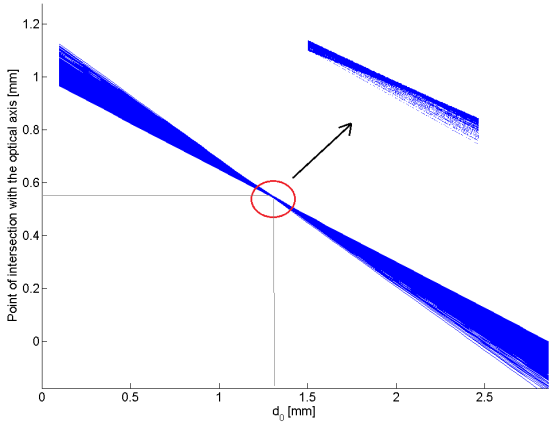

Fig. 5. Distance where the light rays traced back from the water cross the optical axis of the camera depending on d_0. Different lines correspond to different incident angles. It can be noticed that an optimum exist where the focus section is small, i.e., the rays cross in almost a point.

TABLE I

OPTIMAL $d_0^*/{}^v d_0^*$ OF THE CENTERS OF PROJECTION OF THE PHYSICAL/VIRTUAL CAMERA FOR DIFFERENT GLASS THICKNESSES AND SALINITY

d_1 [mm]	$n_w = 1.333$(sweet water)	$n_w = 1.342$(salty water)
1	0.15mm/0.06mm	0.14mm/0.06mm
3	0.45mm/0.18mm	0.42mm/0.17mm
5	0.76mm/0.31mm	0.70mm/0.29mm
10	1.52mm/0.61mm	1.40mm/0.58mm
15	2.28mm/0.92mm	2.10mm/0.87mm
20	3.04mm/1.22mm	2.80mm/1.15mm

as a secondary center of projection placed $0.5851mm$ away from the glass panel, i.e., we define a new *virtual camera* model. For this case, the camera behind the flat glass panel can effectively be treated as an SVP camera and represented with the pinhole model. Sample values of optimal d_0^* of the physical camera and of the resulting center of projection positions ${}^v d_0^*$ of the virtual camera for different thicknesses of the glass panel in sweet and salty water are presented in the Table I.

The typical set-up of underwater cameras where the front end of the lenses are placed as close as possible to the front window corresponds very well to this analysis. These observations lead to the following conclusion: Although the pinhole camera model does not represent the actual physical state, for the purpose of underwater vision it can be used if the distance between the center of projection and glass plane is very small (Fig. 7) by employing a virtual camera with a focal length derived from the axial model. This hypothesis is further substantiated in simulations that are presented and discussed in the following section.

III. SIMULATIONS

For this experiment the following steps were performed. d_1 is assumed to be constant and $d_1 = 10mm$. For different values of d_0, the camera is calibrated with 27 checkerboards in 3D space as presented in Fig. 6; the corner points are

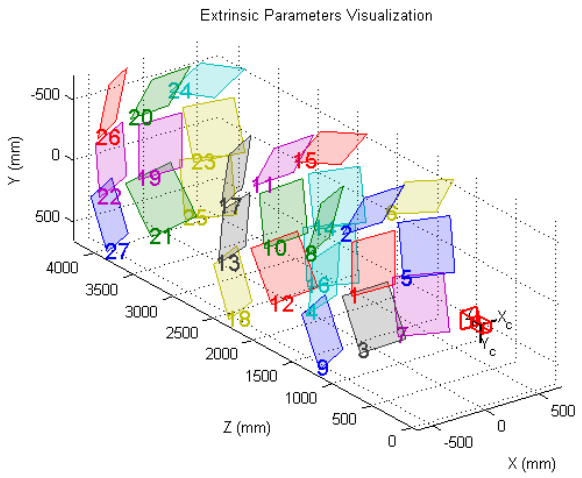

Fig. 6. Positions of the calibration patterns used in the simulations.

projected to the image plane using the full physical model including refraction. This forward projection requires solving a twelve-degree polynomial as presented in [4]. This data is used to calibrate the camera as if it would be underwater.

In the second step, a random set of 100 points is generated in the 3D space in front of the camera. This set is then projected onto the image plane twice for each d_0. Once, the projection is performed with the full physical model to get the expected image coordinates and a second time with camera matrix from calibration using the pinhole model including undistortion. Then the distance between corresponding points, i.e., the reprojection error, is calculated and used to evaluate the pinhole approximation for each d_0. Fig. 7 shows the results by plotting the average distance between corresponding points for the different d_0.

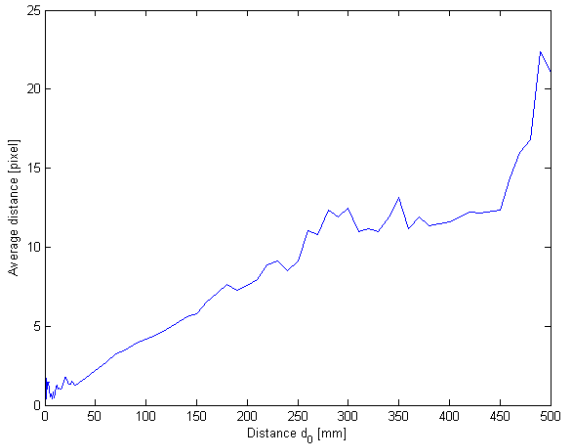

Fig. 7. The reprojection error for changing d_0. Note that for $d_0 = 0\ 10mm$ the errors caused by the SVP approximation can be neglected. The graph is not smooth and may differ from expectations (Fig. 4) because the simulated patterns were not always in the optimal positions for calibration, e.g. they did not always cover the whole field of view of the camera, which is also an effect that can be observed in the real world.

The evaluated values of d_0 reach up to $500mm$ because this is an approximate value that can be found in the literature for experimental setups ([4], [6]). Such big values are used because the refraction effects are then very pronounced and the position of the camera in the housing may be found easily with nonlinear optimization using only pattern observations. While there may be applications for this kind of set-up, e.g., when observing objects in an aquarium and the camera has to keep a substantial clearance to the aquarium wall for some reason, we consider it of very limited interest for underwater cameras where it would be very unusual to have an excessively large housing where the camera is placed half a meter away from the window.

IV. Practical Conclusions

A. Setup assumptions

For the pinax camera model, the following assumptions are made:

- The distance between the glass window and the center of projection of the physical camera is small, i.e., concretely we assume it is in the range of $0 - 10mm$ for negligible errors. For newly designed cameras, the optimal d_0^* can be computed as presented above and taken as design parameter for the housing. For existing cameras, we found the typical set-up of the lenses being close to the window more then sufficient to lead to accurate calibration results.
- The optical axis of the camera is perpendicular to the glass surface. To achieve this a correcting rotation may be applied if needed. This correction is especially important for verged stereo systems behind a single glass panel as discussed in more detail below.
- The glass thickness and its refraction index are known.
- The water refraction index is approximately known from tables, e.g., [12]. It can also be indirectly measured with a CTD sensor, which is used on many vehicles.

Under these assumptions, we can define a virtual camera that follows the pinhole model and has a center of projection ${}^v d_0^*$. Note that ${}^v d_0^*$ is smaller than d_0^* (Tab. I).

B. Underwater stereo camera parameters

The assumptions made about the hardware setup allow to treat a physical camera as if it was in the optimal position with respect to the glass panel without causing significant errors. These assumptions and further knowledge of the intrinsic and extrinsic parameters of the complete physical camera system in air allow to compute the virtual intrinsic and extrinsic parameters for underwater usage. For stereo vision, the images must be corrected to remove lens distortion and refraction, and rectified. The schematic view as applied to a general stereo camera is presented in Fig. 8.

The correction of vergence of the cameras behind a single glass panel is the key topic of this paper. First, the rotation between the two real and the two virtual cameras must be found (R_{right} and R_{left}). To this end, both virtual cameras are defined to have orthogonal optical axes to the glass panel and the Pinax model may be used. However, there is a known rotation between these cameras R that can be determined

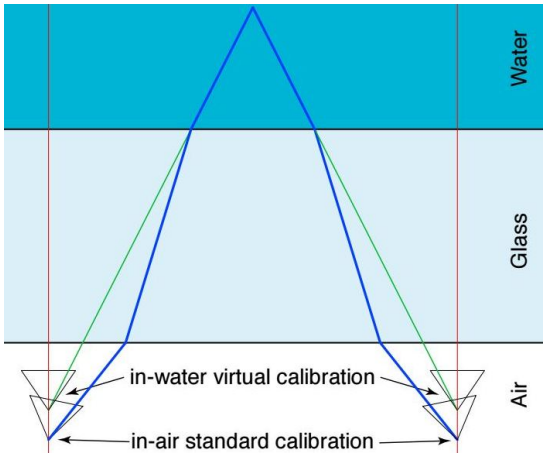

Fig. 8. Real and virtual cameras used in the method.

by in-air calibration. The x axis of the final stereo camera system is defined to be along the translation vector t between the cameras. This ensures that the resulting camera x axes are aligned. The z axis is taken as the average of the two in-air camera optical axes. The y axis is set accordingly to the x and z axes. This defines the rotation matrices for both cameras used later for the image rectification:

$$
\begin{aligned}
x &= -\frac{t}{|t|} \\
a &= \left[\begin{pmatrix} 0 \\ 0 \\ 1 \end{pmatrix} + R \begin{pmatrix} 0 \\ 0 \\ 1 \end{pmatrix} \right] \cdot 0.5 \\
z' &= \frac{a}{|a|} \\
y &= z' \times x \\
z &= x \times y \\
R_{right} &= (x, y, z) \\
R_{left} &= R_{right} R^T
\end{aligned}
$$

Here, R_{right} is constructed by vector concatenation. The transformation (t, R) is assumed to describe the left camera coordinate frame relative to the right. This is equivalent to changing the original Pinax assumption, that the camera axis is orthogonal to the glass panel, to a new assumption: a baseline between the cameras must be parallel to the front glass panel. In most cases, it will be true as even when the cameras are verged they are usually mounted on the same plane for simpler construction.

Once the rotation between the real and virtual cameras is known, the image correction can be computed as derived in [11]. For each pixel of the image from the virtual camera a point is projected into a 3D space at a fixed distance in the operation range, typically a distance of $5m$ is used. Its coordinates are then transformed into the real camera frame and projected to the physical camera image using the refraction model. The resulting image pixel coordinates are then undistorted according to the in-air calibrated lens distortion parameters. This procedure has to be computed only once, and leads to an image transformation for undistortion and rectification that can be stored in a lookup table (Fig. 9).

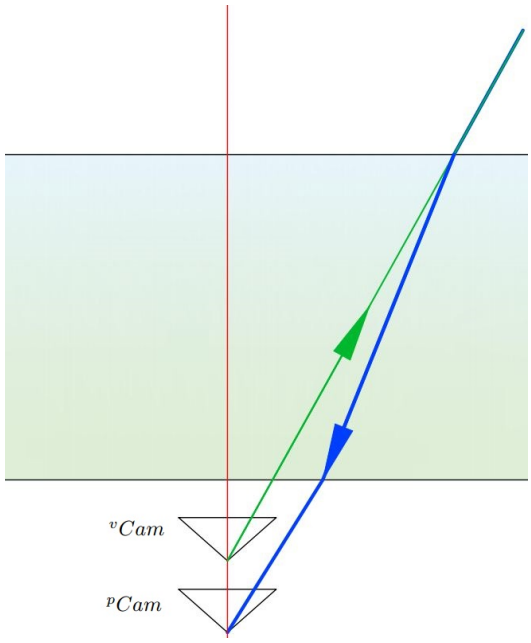

Fig. 9. Calculation of the distortion correction between the virtual Pinax camera ^{v}Cam and the physical camera ^{p}Cam.

V. Real World Experiment and Results

A. Experimental setup

Our method has already been used for different stereo systems on multiple vehicles within the EU FP7-funded projects "Marine robotic system of self-organizing, logically linked physical nodes (MORPH)", "Cognitive Autonomous Diving Buddy (CADDY)" and "Dexterous ROV: effective dexterous ROV operations in presence of communication latencies (DexROV)". Fig. 1 and 2 show two examples of qualitative results of high quality colored point clouds being generated based on in-air calibration with our method of the stereo cameras used in field trials. In this section, we provide a quantitative analysis using a Point Grey Bumblebee XB3 camera closed in a sealed housing (Fig. 10). The cameras were calibrated in-air before mounting them in the housing.

During the experiments, a set of images of a standard calibration pattern was recorded to serve as validation data. The pattern was presented at different distances to the camera such that the test points covered the whole field of view of the camera in an even fashion. This is important: any refraction-based effects are less apparent in the center of the image. In the validation step, pattern points were traced and their 3D arrangement according to the stereo measurements was compared to the ground truth. The error was then normalized by dividing by the distance and is expressed in %. Results are accumulated according to the distance of the camera to the pattern. This test allows to evaluate a metric error of the generated point-cloud depending on the distance to the camera. Then a second test was performed: for a single

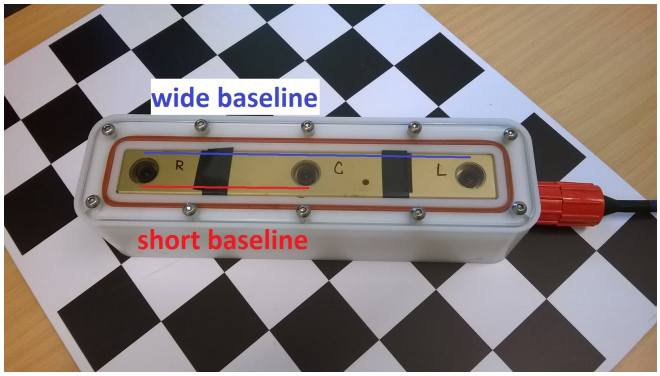

Fig. 10. A Point Grey Bumblebee XB3 camera is used in the experiments. This device features three cameras and can hence be used to test two different stereo camera set-up, namely one with a short and one with a wide baseline.

distance, the y coordinates of corresponding pattern points on the left and right camera images are compared. This test validates the quality of epipolar rectification.

The experiments compare the result of our method presented here with the state of the art method of calibrating in-situ, i.e., underwater, and correcting with a standard pinhole model - see, e.g., [13], [14], [15], [16], [17], [18], [19], [20], [21], [22], [23], [24]. We also include results for the common practice to calibrate the camera in-water only once and then using it in a different setting, e.g., calibrating in a pool and then performing experiments in the sea. We show that this leads to significant further errors in the standard methods.

The computation times of both our method and standard approaches are very similar, respectively even identical as the correction can in both cases be based on very fast look-up table operations suited for real-time processing.

B. Pointgrey Bumblebee XB3 - wide baseline

The first experiment is done with the XB3 wide baseline comparing four correction methods:

1) in-air calibration only,
2) state of the art underwater calibration in the same location as the validation environment, i.e., the same salinity for calibration as for validation (both sweet water),
3) state of the art calibration in salty water and validation in sweet water, and
4) our prediction-based correction method with in-air calibration.

The results are presented in Fig.11. Our prediction based correction with in-air calibration performs the best in terms of accuracy. The in-air calibration with a refraction-less pinhole model leads to many samples that were so significantly distorted that no stereo processing was feasible anymore and metric information could hence not be extracted for these cases. So, the cases where this method performed worst could not be included. The plot for the "in-air calibration" is therefore even too optimistic - though showing the worst performance. It is included only for the sake of illustration purposes. The results also show that the standard process

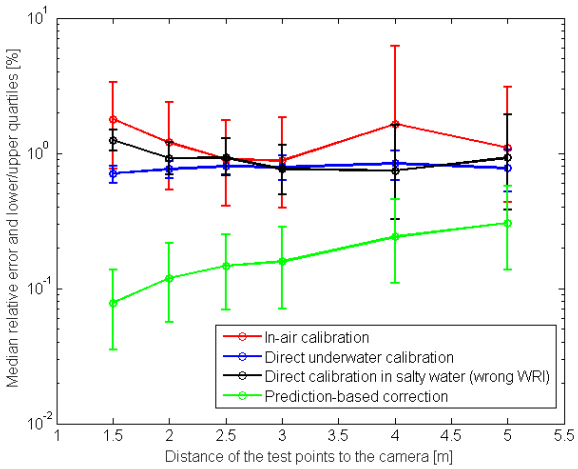

Fig. 11. Relative error of the triangulated points in %. The error bars show the upper and lower quartile values of the error, center dots are medians. The error values are plotted for nominal distance of the calibration pattern during the test. Note that for in-air calibration many samples were too distorted to be processed; therefore the "in-air calibration" is in fact even worse then this plot suggests. Note the log scale on the y axis, used here due to the very high error of the "in-air calibration" case.

of in-water calibration does not only perform worse than our method, it is also strongly depended on environmental conditions. If the camera is for example calibrated in a pool and used in the sea, additional errors are introduced.

C. Pointgrey Bumblebee XB3 - short baseline

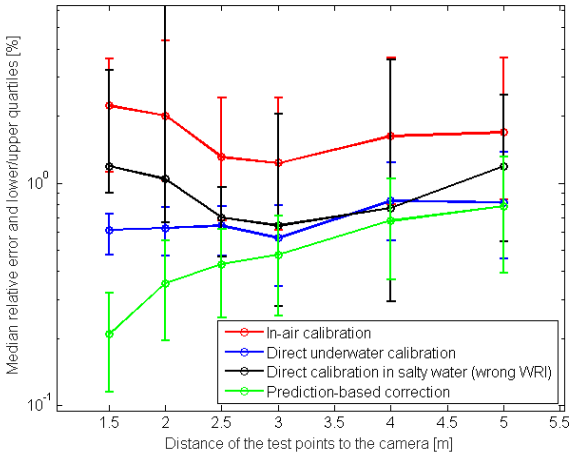

Fig. 12. Relative error of the triangulated points in %. The error bars show the upper and lower quartile values of the error, center dots are medians. The error values are plotted for nominal distance of the test pattern. Note that for in-air calibration many samples were too distorted to be processed, i.e., its performance is even worse than this plot suggests. Also note again the log scale on the y axis.

The same set of experiments was also performed on data recorded with the short baseline stereo-pair of the XB3. The results are plotted in Fig.12. These results further confirm the previous observations. Our prediction based correction with in-air calibration performs the best in terms of accuracy. Even

though the direct underwater calibration could be expected to work best it important to note, that much worse, comparing to in air, underwater light conditions and natural light scattering in water introduce significant noise in the images, leading to worse calibration results.

VI. Conclusions

In this paper an extension to our Pinax model [11] for underwater camera calibration is presented. The Pinax refraction correction method was previously introduced for cameras with optical axes orthogonal to glass panel. But many mass-produced stereo systems are verged, which was treated in this paper. The extended method was tested with real world data showing that the Pinax model can be successfully used for verged stereo vision systems behind a single flat panel.

Acknowledgements

The authors would like to thank Nikola Miskovic and his team from the University of Zagreb for providing the camera housing used in the experiments. The research leading to the presented results was supported in part by the European Community's Seventh Framework Programme under grant agreements: n. 288704 "Marine robotic system of self-organizing, logically linked physical nodes (MORPH)", n. 611373 "Cognitive Autonomous Diving Buddy (CADDY)", and n. 635491 "Dexterous ROV: effective dexterous ROV operations in presence of communication latencies (DexROV)".

References

[1] J. Horgan and D. Toal, "Review of machine vision applications in unmanned underwater vehicles," in *Control, Automation, Robotics and Vision, 2006. ICARCV '06. 9th International Conference on*, Dec 2006, pp. 1–6.

[2] C. Kunz and H. Singh, "Hemispherical refraction and camera calibration in underwater vision," in *OCEANS 2008*, Sept 2008, pp. 1–7.

[3] V. Chari and P. F. Sturm, "Multi-view geometry of the refractive plane." in *BMVC*. British Machine Vision Association, 2009.

[4] A. Agrawal, S. Ramalingam, Y. Taguchi, and V. Chari, "A theory of multi-layer flat refractive geometry," in *Computer Vision and Pattern Recognition (CVPR), 2012 IEEE Conference on*, June 2012, pp. 3346–3353.

[5] P. Sturm, "Multi-view geometry for general camera models," in *Computer Vision and Pattern Recognition, 2005. CVPR 2005. IEEE Computer Society Conference on*, vol. 1, June 2005, pp. 206–212 vol. 1.

[6] T. Treibitz, Y. Schechner, C. Kunz, and H. Singh, "Flat refractive geometry," *Pattern Analysis and Machine Intelligence, IEEE Transactions on*, vol. 34, no. 1, pp. 51–65, Jan 2012.

[7] J. Gedge, M. Gong, and Y.-H. Yang, "Refractive epipolar geometry for underwater stereo matching," in *Computer and Robot Vision (CRV), 2011 Canadian Conference on*, May 2011, pp. 146–152.

[8] R. Li, H. Li, W. Zou, R. Smith, and T. Curran, "Quantitative photogrammetric analysis of digital underwater video imagery," *Oceanic Engineering, IEEE Journal of*, vol. 22, no. 2, pp. 364–375, Apr 1997.

[9] X. Chen and Y.-H. Yang, "Two-view camera housing parameters calibration for multi-layer flat refractive interface," in *Computer Vision and Pattern Recognition (CVPR), 2014 IEEE Conference on*, June 2014, pp. 524–531.

[10] A. Jordt-Sedlazeck and R. Koch, "Refractive calibration of underwater cameras," in *Proceedings of the 12th European Conference on Computer Vision - Volume Part V*, ser. ECCV'12, 2012, pp. 846–859.

[11] T. Łuczyński, M. Pfingsthorn, and A. Birk, "The pinax-model for accurate and efficient refraction correction of underwater cameras in flat-pane housings," *Ocean Engineering*, vol. 133, pp. 9 – 22, 2017. [Online]. Available: http://www.sciencedirect.com/science/article/pii/S0029801817300434

[12] W. Roswell, A. Halikas, and G. Halikas, "The index of refraction of seawater - technical report," *University of California, San Diego Visibility Laboratory*, 1976.

[13] M. R. Shortis and E. S. Harvey, "Design and calibration of an underwater stereo-video system for the monitoring of marine fauna populations," *International Archives of Photogrammetry and Remote Sensing*, vol. 32, no. 1, 1998.

[14] N. Gracias and J. Santos-Victor, "Underwater video mosaics as visual navigation maps," *Computer Vision and Image Understanding*, vol. 79, no. 1, pp. 66–91, 2000.

[15] N. Pessel, J. Opderbecke, and M.-J. Aldon, "Camera self-calibration in underwater environment," in *11th International Conference in Central Europe on Computer Graphics, Visualization and Computer Vision*, 2003.

[16] O. Pizarro, R. Eustice, and H. Singh, "Relative pose estimation for instrumented, calibrated imaging platforms," in *Proceedings of Digital Image Computing Techniques and Applications*, 2003, pp. 601–612.

[17] S. Negahdaripour, C. Barufaldi, and A. Khamene, "Integrated system for robust 6-dof positioning utilizing new closed-form visual motion estimation methods in planar terrains," *Oceanic Engineering, IEEE Journal of*, vol. 31, no. 3, pp. 533–550, 2006.

[18] S. Negahdaripour, H. Sekkati, and H. Pirsiavash, "Opti-acoustic stereo imaging, system calibration and 3-d reconstruction," in *Computer Vision and Pattern Recognition, 2007. CVPR '07. IEEE Conference on*, 2007, pp. 1–8.

[19] V. Brandou, A. Allais, M. Perrier, E. Malis, P. Rives, J. Sarrazin, and P. Sarradin, "3d reconstruction of natural underwater scenes using the stereovision system iris," in *OCEANS 2007 - Europe*, june 2007, pp. 1 –6.

[20] A. Sedlazeck, K. Koser, and R. Koch, "3d reconstruction based on underwater video from rov kiel 6000 considering underwater imaging conditions," in *OCEANS 2009 - EUROPE*, may 2009, pp. 1 –10.

[21] M. Johnson-Roberson, O. Pizarro, S. B. Williams, and I. Mahon, "Generation and visualization of large-scale three-dimensional reconstructions from underwater robotic surveys," *Journal of Field Robotics*, vol. 27, no. 1, pp. 21–51, 2010.

[22] C. Kunz and H. Singh, "Stereo self-calibration for seafloor mapping using auvs," in *Autonomous Underwater Vehicles (AUV), 2010 IEEE/OES*, Sept 2010, pp. 1–7.

[23] C. Beall, F. Dellaert, I. Mahon, and S. B. Williams, "Bundle adjustment in large-scale 3d reconstructions based on underwater robotic surveys," in *OCEANS, 2011 IEEE - Spain*, 2011, pp. 1–6.

[24] L. Kang, L. Wu, and Y.-H. Yang, "Experimental study of the influence of refraction on underwater three-dimensional reconstruction using the svp camera model," *Appl. Opt.*, vol. 51, no. 31, pp. 7591–7603, Nov 2012.